crystals

MDPI

Article

# Syntheses, Crystal Structure and Magnetic Properties of $Tl_9RETe_6$ (*RE* = Ce, Sm, Gd)

**Anna Isaeva [1,2], Rico Schönemann [3,†] and Thomas Doert [4,*]**

1 Faculty of Physics, Technische Universität Dresden, D–01062 Dresden, Germany; anna.isaeva@tu-dresden.de
2 Leibniz Institute for Solid State Research, IFW Dresden, D–01069 Dresden, Germany
3 Hochfeld-Magnetlabor (HLD-EMFL), Helmholtz-Zentrum Dresden Rossendorf, D–01328 Dresden, Germany; rschoenemann@lanl.gov
4 Faculty of Chemistry and Food Chemistry, Technische Universität Dresden, D–01062 Dresden, Germany
* Correspondence: thomas.doert@tu-dresden.de; Tel.: +49-351-463-33864
† Present address: MPA-MAGLAB, Los Alamos National Laboratory, Los Alamos, NM 87545, USA.

Received: 17 March 2020; Accepted: 2 April 2020; Published: 7 April 2020


**Abstract:** The three compounds $Tl_9RETe_6$ with *RE* = Ce, Sm, Gd were synthesized from the elements at 1020 K. Their isostructural crystal structures are ordered derivatives of the $Tl_5Te_3$ type with rare-earth metal and thallium occupying different Wyckoff positions. The structures can be understood as charge-ordered in accordance with the Zintl-Klemm concept: 9 $Tl^+$ + $RE^{3+}$ + 6 $Te^{2-}$. DFT calculations for $Tl_9GdTe_6$, however, result in a low, but finite density of states at the Fermi level. Magnetic data confirm trivalent Gd, but indicate a small amount of $Ce^{4+}$ in $Tl_9CeTe_6$; no indications for long-range magnetic order was found down to $T$ = 2 K.

**Keywords:** Tellurides; thallium; rare-earth metals; crystal structure; magnetic properties

## 1. Introduction

$Tl_5Te_3$ and its derivatives have attracted considerable attention as thermoelectric materials [1–11] and recently as topological materials with a superconducting phase below 2.4 K [12]. Binary $Tl_5Te_3$ is known to adopt the $In_5Bi_3$ type structure (space group *I*4/*mcm*, *a* = 893.0(2) pm, *c* = 1258.9(4) pm), with two distinct Tl positions (Tl1 on Wyckoff site 4*c* and Tl2 on 16*l*) and two Te positions (Te1 on 4*a*, Te2 on 8*h*) [12,13]. Several ternary derivatives of the types $Tl_9MTe_6$ (*M* = Sb, Bi), $Tl_9RETe_6$ (*RE* = rare earth metal) and $Tl_4M'Te_3$ (*M*′ = Cu, Sn, Pb, Mo) have been reported [1–11,14–21]. Substitutions have generally been found to occur on Wyckoff site 4*c* preferably. The composition $Tl_4M'Te_3$ could in principle be realized by complete substitution of Tl1 on Wyckoff site 4*c*, the composition $Tl_9MTe_6$ corresponds to a substitution of one-half of the Tl1 atoms. Mixed *M*/Tl occupancies on the 4*c* site were reported for $Tl_{10-x}RE_xTe_6$ (*RE* = La, Ce, Pr, Nd, Sm, Gd, Tb, Dy, Ho and Er, with $0 < x < 1.32$), e.g., [6,9]. Magnetization data for the compounds $Tl_{10-x}RE_xTe_6$, *RE* = Ce, Pr, Tb, Sm point at paramagnetic behavior in low fields down to $T$ = 2 K and the extracted effective paramagnetic moments indicate (with the exception of Ce) trivalent rare earth metals [10]. Therefore, a charge ordered formula for the composition $Tl_9RETe_6$ could be written as 9 $Tl^+$ + $RE^{3+}$ + 6 $Te^{2-}$ in accordance with the semiconducting properties of these compounds [9]. Moreover, it may as well give rise to the formation of a two-fold superstructure with full ordering of $M^{3+}$ and $Tl1^+$ atoms.

The progenitor of the series $Tl_5Te_3$ has a non-trivial topology of the electronic band structure due to a band inversion between the Tl2 and Te states of opposite parity at the *Z* point of the 3D Brillouin zone [12]. Given the current interest in quantum materials that combine non-trivial topology and intrinsic magnetic order [22], we re-investigated the crystal structures and magnetic properties of $Tl_9RETe_6$ with *RE* = Ce, Sm, Gd on single crystals. Such compound in a magnetically ordered state

would be a candidate magnetic topological semimetal. We aim to provide the crystallographic data of highest possible quality and precision for the first-principles calculations, since topological properties depend on the fine details of lattice symmetries. The results are presented in the following.

## 2. Materials and Methods

### *2.1. Synthesis*

All preparation steps were carried out in an argon (99.996% Messer-Griesheim, Sulzbach, Germany) filled glovebox (MBraun, Garching, Germany). The title compounds were obtained by direct synthesis of the elements in stoichiometric amounts, typically aiming at a sample mass of 1.5 g per batch. The rare-earth metals (Ce, Gd, Sm: 99.9%, Strem, Kehl, Germany) were rasped from compact blocks and Tl (99.9% Alfa Aesar, Karlsruhe, Germany) was cut from a rod. The metal pieces were filled in silica ampoules with glassy carbon crucibles together with the calculated amount of Te (lump 99.999%, Alfa Aesar, Karlsruhe, Germany). The ampoules were flame sealed and placed in a furnace, heated to 1020 K for 24 h and cooled to ambient temperature with 5 K/h.

The resulting ingots are dark-grey with metallic luster. The materials are brittle and can easily be crushed. Some parts were further ground for powder X-ray and magnetic measurements. Crystals for structure determination could be selected from the crushed ingots.

### *2.2. X-ray Powder Diffraction*

X-ray powder diagrams (powder diffractometer XPert Pro, PANalytical GmbH, Kassel, Germany; CuK$\alpha_1$ radiation, Bragg-Brentano setup) were recorded to check for phase purity and to determine the lattice parameters. Moreover, Rietveld fits were performed to refine the lattice parameters and to check the structure model derived from single crystal data for consistency [23].

### *2.3. Energy Dispersive X-ray Spectroscopy (EDX)*

Energy dispersive X-ray (EDX) analyses were performed in a SEM SU 8020 (Hitachi High-Technologies Europe GmbH, Krefeld, Germany) equipped with a silicon drift EDX detector XMAX$^N$ (Oxford Instruments, Wiesbaden, Germany) at 30 kV acceleration voltage. Crystals of the phase pure samples were embedded in a conductive polymer matrix, cut and polished to provide a plane and clean surface. Analyses were made by averaging on several points and line scans of different crystals for each sample according to the fundamental parameter method applying a PAP matrix correction [24].

### *2.4. Crystal Structure Determination*

Single crystal experiments were performed on a Kappa Apex II CCD diffractometer (Bruker-AXS GmbH, Karlsruhe, Germany) with Mo *K*$\alpha$ radiation using the software package Apex Suite [25]. A multi-scan absorption correction was employed [26]. Atom parameters and atom designations for structure refinement with Jana 2006 [23] were derived by the symmetry reduction stated in the Discussion, see below. Diamond 4 was used for structure visualization [27].

### *2.5. Electronic Structure Calculations*

Density functional theory (DFT) calculations within the local density approximation with Hubbard correction (LDA+*U*) using the around mean field (AFM) double counting were performed for $Tl_9GdTe_6$ in the full-potential full-electron linear augmented plane-wave (FP-LAPW) code [28]. Spin-orbit coupling was taken into account fully-relativistically. The values of Hubbard $U$ = 6.7 eV and $J$ = 0.7 eV were chosen to treat the Gd d-orbitals. These optimized parameters were reported for the electronic structure of pure gadolinium metal and we tested them to reproduce the magnetic moments on Gd atoms with our program code [29]. Formal charges were calculated according to the Bader partitioning scheme [30].

### 2.6. Magnetic Measurements

Magnetization measurements on sample of $Tl_9CeTe_6$ and $Tl_9GdTe_6$ were carried out with a commercial superconducting quantum interference device (SQUID) magnetometer MPMS (Quantum Design Europe, Darmstadt, Germany) in a temperature range of 300 K ≤ $T$ ≤ 2 K.

## 3. Results and Discussion

EDX analyses performed on several of the as-grown crystals of each sample confirm the composition of the compounds within the limit of the method, although a slight excess of Te was observed for all samples, Table 1. No hints for contaminations or defects were obtained.

**Table 1.** Energy dispersive X-ray (EDX) derived composition of $Tl_9RETe_6$ (atom-%), stated are average values from different crystals of each sample.

| Element | $Tl_9CeTe_6$ | $Tl_9SmTe_6$ | $Tl_9GdTe_6$ | Theor. |
|---|---|---|---|---|
| *RE* | 5.7(4) | 5.9(4) | 6.4(2) | 6.2 |
| Tl | 56.0(3) | 55.3(5) | 55.1(3) | 56.3 |
| Te | 38.3(3) | 38.8(2) | 38.5(4) | 37.5 |

According to the X-ray powder patterns and the respective Rietveld fits, phase-pure samples of $Tl_9CeTe_6$, $Tl_9SmTe_6$ and $Tl_9GdTe_6$ were obtained, cf. Figure 1 as an example and also Figure S1. The tetragonal lattice parameters derived from powder X-ray data are in good agreement with those from single crystal experiments (Table 2).

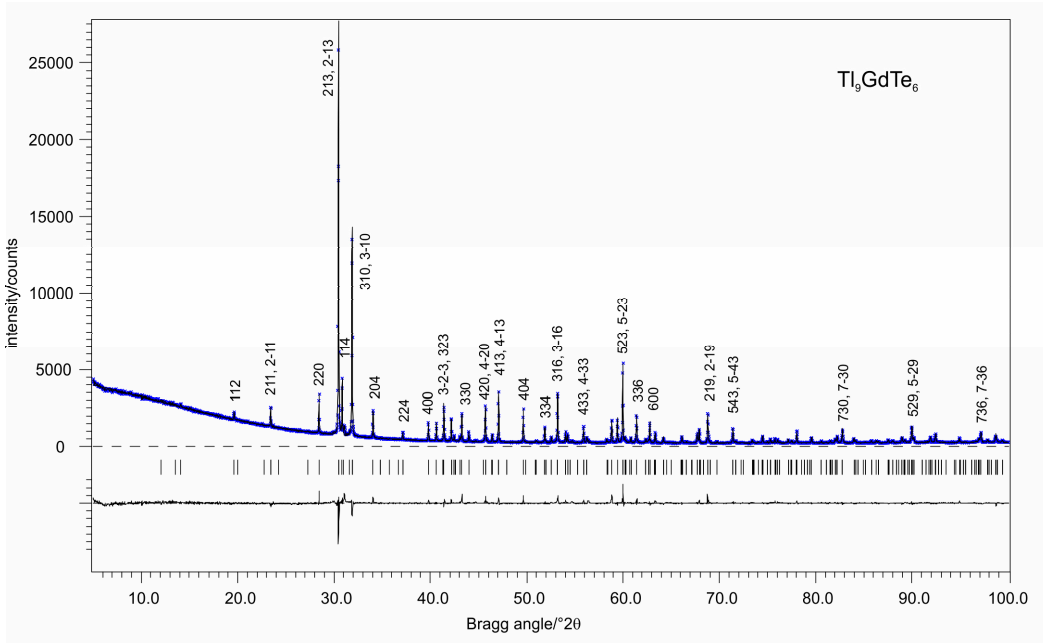


**Figure 1.** Experimental X-ray powder data (black) and Rietveld fit (blue line) for $Tl_9GdTe_6$ as example; the positions of the Bragg reflections and the difference plot are shown in the lower part; CuK$\alpha_1$, λ = 1.54051 Å. Profile $R$ factors: $GOF$ = 1.84, $R_p$ = 3.81 $wR_p$ = 6.08.

Analyses of the single-crystal data sets of the compounds $Tl_9CeTe_6$, $Tl_9SmTe_6$ and $Tl_9GdTe_6$ indicated body-centered tetragonal unit cells each. For all three compounds, a considerable number of reflections with intensities well above a threshold of 3$\sigma(I)$ were found to contradict glide planes and screw axes. Moreover, depending on the twin volume ratio (cf. below), the $R_{int}$ value for symmetry averaging was found to be significantly lower for *Laue* class 4/*m* as compared to *Laue* class 4/*mmm*

(e.g., 0.071 vs. 0.125, respectively, for $Tl_9SmTe_6$). These findings refute space group *I*4/*mcm* and point towards *I*4/*m* instead.

Structure solutions were hence made in *I*4/*m* and refinements proceeded smoothly to the results and residuals stated in Table 2. Space group *I*4/*m* provides a possibility for $Tl^+$ and $RE^{3+}$ ions to reside on two crystallographically independent sites, as has been described for $SbTl_9Te_6$ in a similar way [20]. The symmetry and structure relations between $Tl_5Te_3$ in space group *I*4/*mcm* and those of the title compounds $Tl_9RETe_6$ (*RE* = Ce, Sm, Gd) is depicted in the Bärnighausen diagram in Figure 2. The occupancies of the Tl1 (Wyckoff site 2*a*) and the *RE* atoms (2*b*) were found to be unity within an uncertainty interval of 3$\sigma$ in the refinements. No experimental evidence for a mixed occupancy on the 2*a* and 2*b* sites was found, as for any other Wyckoff site. The main crystallographic data and refinement details are stated in Tables 2 and 3, selected interatomic distances are listed in Table 4. Crystallographic data have been deposited with the Fachinformationszentrum Karlsruhe, D-76344 Eggenstein-Leopoldshafen (Germany) and can be obtained on quoting the depository number CSD-427736 ($Tl_9CeTe_6$), CSD-427737 ($Tl_9GdTe_6$) and CSD-427738 ($Tl_9SmTe_6$). Note, that despite the evidence of the reflection conditions refuting the higher symmetric space group *I*4/*mcm*, refinements in this space group were performed for reasons of comparison with previously published data. These refinements, as can be seen from Table S1, Supporting Information, resulted in unsatisfactory *R*-values and much higher difference Fourier peaks in all three cases and underline the correct choice of space group *I*4/*m* additionally.

**Table 2.** Crystallographic data and refinement parameters of $Tl_9RETe_6$.

| **Chemical Composition** | **$Tl_9CeTe_6$** | **$Tl_9SmTe_6$** | **$Tl_9GdTe_6$** |
|---|---|---|---|
| $M_r$/g·mol$^{-1}$, *F*(000) | 2745.1, 2189 | 2755.4, 2206 | 2762.3, 2210 |
| temperature/K | | 295(1) | |
| diffractometer type | | Kappa Apex II CCD (Bruker-AXS) | |
| wavelength/Å | | 0.71069 (Mo *Kα*, graphite monochromator) | |
| crystal system | | tetragonal | |
| space group (No.), *Z* | | *I*4/*m* (no. 87), 2 | |
| cell parameters *, *a*/pm | 890.48(2) | 886.50(5) | 887.00(3) |
| *c*/pm | 1313.42(5) | 1306.41(8) | 1306.56(5) |
| cell volume/10$^6$ pm$^3$ | 1041.48(5) | 1026.7(1) | 1027.96(6) |
| density/g·cm$^{-3}$ | 8.75 | 8.91 | 8.92 |
| Abs. coefficient/mm$^{-1}$ | 79.69 | 81.48 | 81.75 |
| absorption correction | | multi-scan (SADABS [26]) | |
| - | 0.289/0.749 | 0.292/0.746 | 0.499/0.747 |
| crystal size / mm$^3$ | 0.189 × 0.057 × 0.045 | 0.021 × 0.027 × 0.043 | 0.075 × 0.061 × 0.035 |
| measurement range | $2.8 \le \theta \le 42.6$<br>$-13 \le h \le 15$<br>$-15 \le k \le 15$<br>$-15 \le l \le 24$ | $2.8 \le \theta \le 34.7$<br>$-11 \le h \le 14$<br>$-9 \le k \le 14$<br>$-20 \le l \le 20$ | $2.8 \le \theta \le 35.2$<br>$-14 \le h \le 13$<br>$-14 \le k \le 11$<br>$-17 \le l \le 19$ |
| $R_{int}$ | 0.0328 | 0.071 | 0.030 |
| refinement | | JANA2006, full-matrix least squares on $F^2$ [23] | |
| reflections, with $I > 3\sigma(I)$, parameters | 1693, 1458, 25 | 1153, 795, 24 | 1151, 830, 25 |
| extinction parameter | 0.118(2) | - | 0.0059(7) |
| goodness-of-fit | 1.5 | 1.1 | 1.2 |
| $R_1$(obs), $wR_2$(obs) | 0.031, 0.065 | 0.035, 0.062 | 0.026, 0.049 |
| $R_1$(all), $wR_2$(all) | 0.038, 0.066 | 0.059, 0.069 | 0.050, 0.055 |
| twin matrix | | 0 1 0, 1 0 0, 0 0 −1 | |
| twin volume fraction | 0.518(2) | 0.672(2) | 0.997(1) |
| $\Delta\rho_{min}$ / $\Delta\rho_{max}$, e/10$^6$ pm$^3$ | 2.57/−2.02 | 2.02/−3.38 | 2.29/−2.12 |

* from powder data

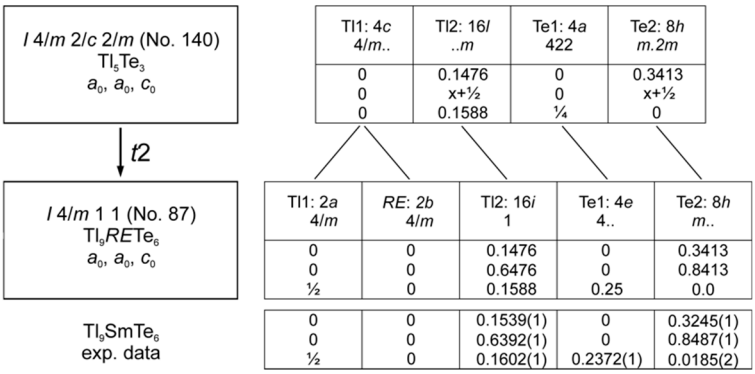


**Figure 2.** Bärnighausen diagram showing the symmetry relationship between the binary $Tl_5Te_3$ [14] and the $Tl_9RETe_6$ title compounds.

As the three title compounds $Tl_9CeTe_6$, $Tl_9SmTe_6$ and $Tl_9GdTe_6$ are isotypic, the structure description and discussion are exemplified by $Tl_9SmTe_6$. The structures of $Tl_5Te_3$ and some of its derivatives have been discussed in several publications; however, authors have emphasized different structural details. Focus was laid on the stacking of two different sets of interpenetrating nets [14], equidistant linear Tl1–Te1 chains running along [001] [14], coordination polyhedra around Tl1 and Te1 [15–21] or a perovskite-like arrangement of $Tl1Te_6$-octahedra in which the large voids are occupied by $Tl_4$-tetrahedra [12]. Figure 3 shows projections of the unit cells of $Tl_9SmTe_6$ and $Tl_5Te_3$ next to each other for comparison. As can be seen, the major difference is in the decoration of the metal sites (Tl1 and *RE*), other structural differences are hardly noticeable from this image.

**Table 3.** Fractional coordinates and isotropic displacement parameters of $Tl_9RETe_6$.

| Atom | *x* | *y* | *z* | $U_{eq}$, pm$^2$ |
|---|---|---|---|---|
| | | **$Tl_9CeTe_6$** | | |
| Ce | 0 | 0 | 0 | 170(1) |
| Tl1 | 0 | 0 | 1/2 | 252(1) |
| Tl2 | 0.1557(1) | 0.6377(1) | 0.1600(1) | 335(1) |
| Te1 | 0 | 0 | 0.2403(1) | 120(1) |
| Te2 | 0.3284(1) | 0.8466(1) | 0 | 180(1) |
| | | **$Tl_9SmTe_6$** | | |
| Sm | 0 | 0 | 0 | 173(3) |
| Tl1 | 0 | 0 | 1/2 | 0273(3) |
| Tl2 | 0.1539(1) | 0.6392(1) | 0.1602(1) | 339(1) |
| Te1 | 0 | 0 | 0.2372(1) | 201(3) |
| Te2 | 0.3245(1) | 0.8487(1) | 0 | 185(2) |
| | | **$Tl_9GdTe_6$** | | |
| Gd | 0 | 0 | 0 | 173(3) |
| Tl1 | 0 | 0 | 1/2 | 273(3) |
| Tl2 | 0.1539(1) | 0.6392(1) | 0.1602(1) | 339(1) |
| Te1 | 0 | 0 | 0.2372(1) | 201(3) |
| Te2 | 0.3245(1) | 0.8487(1) | 0 | 185(2) |

$U_{eq}$ is defined as 1/3 of the orthogonalized $U_{ij}$ tensor.

A more detailed view on the structures, especially on the $Tl1Te_6$ and $SmTe_6$ octahedra, however, reveals further differences. The $Tl1Te_6$ octahedra are defined by two apical Tl–Te distances of 343.3(1) pm and four basal ones of 346.0(1) pm. The Sm atom does also reside in a slightly compressed octahedron with two apical Sm–Te distances of 302.9(1) pm and four basal ones of 317.5(1) pm. The average Sm–Te distances in the octahedra is 312.6(1) pm and thus about 10% shorter than the

average Tl1–Te distance of 345.1(1) pm for the $Tl1Te_6$ octahedra. For comparison: the $Tl1Te_6$ octahedron in the binary phase $Tl_5Te_3$ consists of two apical Tl–Te distances of 314.7 pm and four basal ones of 336.1 pm, resulting in an average value of 329.0 pm; for the $Tl_9RETe_6$ compounds, the average distances in the *RE*–Te and Tl1–Te octahedra are 320.4(1) pm and 343.3(1) pm for $Tl_9CeTe_6$ 314.4(1) pm and 345.9(1) pm for $Tl_9GdTe_6$, respectively. Figure 4 illustrates the size difference by enfolding the octahedra with a sphere of the radius of the average Sm–Te and Tl1–Te distances. This spherical representation clearly evidences why the ternary compounds preferably adopt the lower symmetric structure in *I*4/*m*. In this context, the term "charge-ordered structure" does not reflect the whole truth as size-order is at least a comparable driving force.

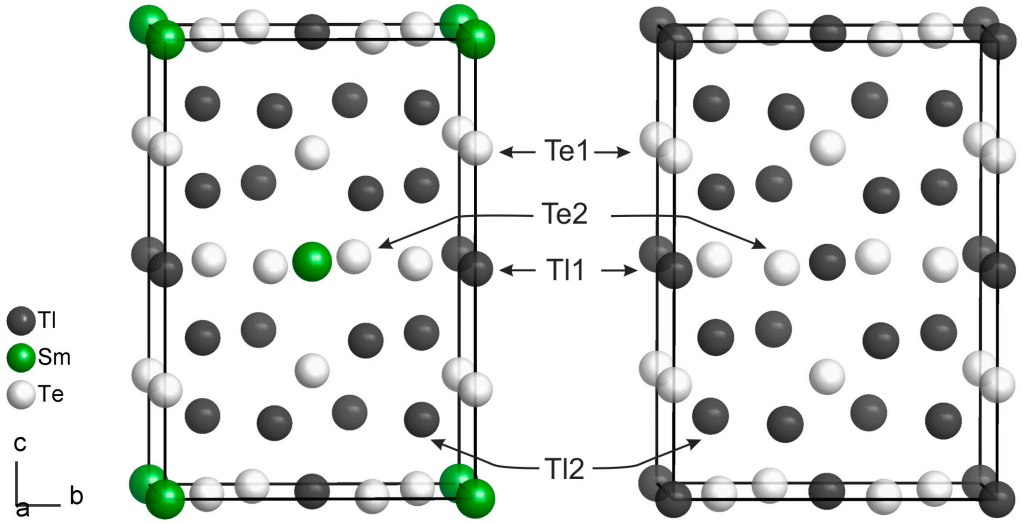


**Figure 3.** View on the unit cells of $Tl_9SmTe_6$ (left) and $Tl_5Te_3$ (right, [14]).

Looking for next nearest neighbors of the Sm and Tl1 atoms, eight Tl2 atoms forming a cuboid have to be considered. The distances to the central Sm and Tl1 atoms are 409.2(1) pm and 391.3(1) pm, respectively. The Te1 atoms are surrounded by a square antiprism of eight Tl2 atoms with both square faces capped by Tl1 or Sm atoms, Figure 5.

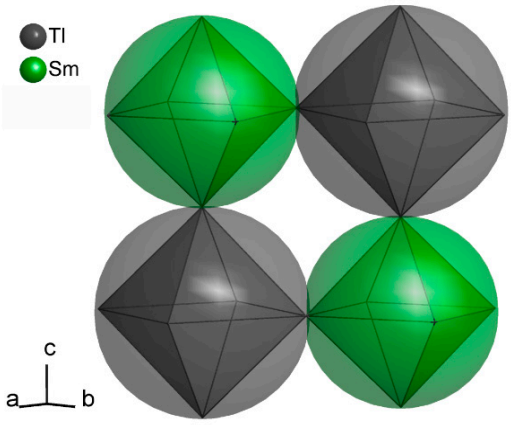


**Figure 4.** Size difference of the $SmTe_6$ (green) and $Tl1Te_6$ (dark grey) octahedra; the radius of a sphere is the average distance to the coordinating Te atoms.

**Table 4.** Selected interatomic distances (pm) of $Tl_9RETe_6$.

| | | | | | | | |
|---|---|---|---|---|---|---|---|
| **$Tl_9CeTe_6$** | | | | | | | |
| Ce– | Te1 | 315.7(1) | 2× | Tl1– | Te1 | 341.1(1) | 2× |
| | Te2 | 322.8(1) | 4× | | Te2 | 344.4(1) | 4× |
| | Tl2 | 409.2(1) | 8× | | Tl2 | 391.4(1) | 8× |
| Tl2– | Tl2 | 352.3(1) | | Tl2– | Te2 | 320.0(1) | |
| | | 352.8(1) | 2× | | | 346.4(1) | |
| | | 370.2(1) | | | | 347.6(1) | |
| | Te1 | 355.2(1) | | | | | |
| | | 366.6(1) | | | | | |
| **$Tl_9SmTe_6$** | | | | | | | |
| Sm– | Te1 | 309.9(1) | 2× | Tl1– | Te1 | 343.3(1) | 2× |
| | Te2 | 317.5(1) | 4× | | Te2 | 346.0(1) | 4× |
| | Tl2 | 405.9(1) | 8× | | Tl2 | 391.3(1) | 8× |
| Tl2– | Tl2 | 350.2(1) | | Tl2– | Te2 | 318.1(1) | |
| | | 350.3(1) | 2× | | | 343.6(1) | |
| | | 362.0(1) | | | | 348.7(1) | |
| | Te1 | 356.8(1) | | | | | |
| | | 362.0(1) | | | | | |
| **$Tl_9GdTe_6$** | | | | | | | |
| Gd– | Te1 | 309.4(1) | 2× | Tl1– | Te1 | 343.9(1) | 2× |
| | Te2 | 316.9(1) | 4× | | Te2 | 346.9(1) | 4× |
| | Tl2 | 405.7(1) | 8× | | Tl2 | 392.0(1) | 8× |
| Tl2– | Tl2 | 350.1(1) | | Tl2– | Te2 | 318.2(1) | |
| | | 350.4(1) | 2× | | | 343.1(1) | |
| | | 368.2(1) | | | | 349.7(1) | |
| | Te1 | 357.6(1) | | | | | |
| | | 361.5(1) | | | | | |

$Tl_5Te_3$, $Tl_5Se_3$ and their ternary derivatives can, at least formally, be written on the basis of a Zintl-like charge-ordered formula in the first approach. For the rare-earth metal substituted compounds $Tl_9RETe_6$, this would result in 9 $Tl^+$ + $RE^{3+}$ + 6 $Te^{2-}$. The sizes of the metal coordination octahedra can then be rationalized according to the ionic radii of the respective $Tl^+$ and $RE^{3+}$ metal ions: 164 pm for $Tl^+$, 115 pm for $Ce^{3+}$, 110 pm for $Sm^{3+}$ and 108 pm for $Gd^{3+}$, all for octahedral coordination [31]. The smaller $TlTe_6$ coordination polyhedron in $Tl_5Te_3$ as compared to those in $Tl_9RETe_6$ is also understandable: In $Tl_5Te_3$ one fifth of the Tl atoms (i.e., the Tl atoms on 4*c* in space group *I*4/*mcm*) can be considered to be in an intermediate 2+ valence state: 4 $Tl^+$ + $Tl^{2+}$ + 3 $Te^{2-}$ [32]. However, the formulation as mixed-valent compound according to 9 $Tl^+$ + $Tl^{3+}$ + 6 $Te^{2-}$ is conceivable, yet not supported by crystallographic evidence.

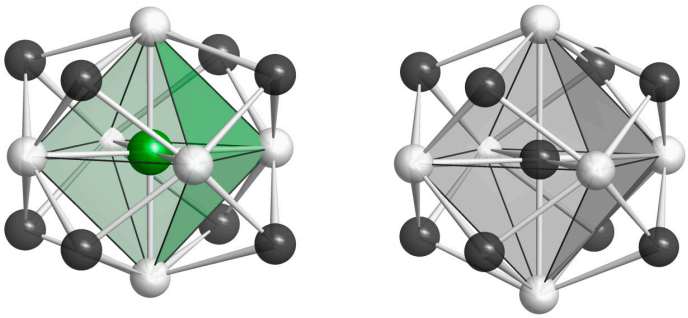

**Figure 5.** Extended coordination polyhedra for Sm (left) and Tl1 atoms (right): slightly compressed $Te_6$ octahedra plus $Tl_8$ cuboid.

Based on the crystallographic data, we perform preliminary spin-polarized band-structure calculations for $Tl_9GdTe_6$ and find that a ferromagnetically ordered state is more energetically favorable than a non-magnetic configuration. Figure 6 shows the full-relativistic bulk electronic spectrum, which is metallic with low yet finite electron density at the Fermi energy. This is in line with the experimentally observed electronic conductivity [8]. At about 0.2 eV below the Fermi level the electron density drops to almost zero and there is an (avoided) band crossing at the Γ point. This feature is constituted by Tl and Te states, while the majority of Gd *f*-states reside at ca. −10 eV. These spin-polarized bands may either hybridize and open a tiny gap or form a protected crossing. In both cases, $Tl_9GdTe_6$ could be a candidate topological material: either a topological insulator or a topological semimetal. These scenarios call for further in-depth elucidation. The calculated effective magnetic moment amounts to 7.4 $\mu_B$/Gd atom. This value is slightly lower than the theoretical moment of 7.98 $\mu_B$ for $Gd^{3+}$ [33], the discrepancy likely pointing towards a certain degree of electron delocalization in a metallic system. The computed formal charges are: Tl1: +0.3, Tl2: +0.3, Gd: +0.55, Te1: −0.5, Te2: −0.5.

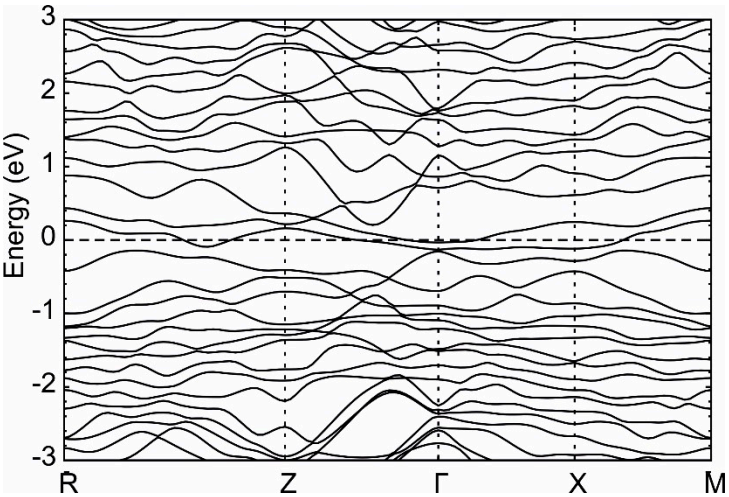


**Figure 6.** Full-relativistic spin-polarized band structure of $Tl_9GdTe_6$.

Magnetic measurements performed on samples of $Tl_9CeTe_6$ (Figure S2) and $Tl_9GdTe_6$ (Figure 7) demonstrate that both compounds are paramagnetic in the temperature interval 2 K < $T$ < 300 K and no long-range magnetic order was established. The Curie–Weis fit for $Tl_9CeTe_6$ results in a magnetic moment of 2.18 $\mu_B$ per Ce-atom, in accordance with [10]. The values are slightly reduced with respect to the expected value of 2.51 $\mu_B$ for a pure $Ce^{3+}$ ($J$ = 5/2) system [33] and might point towards a small amount of $Ce^{4+}$. For $Tl_9GdTe_6$, the Curie–Weis fit yields 8.12 $\mu_B$ per Gd atom for the Gd compound in reasonable agreement with the expected value for a $J$ = 7/2 system of 7.98 $\mu_B$ [33]. Whereas binary $Tl_5Te_3$ turns superconducting at $T_c$ = 2.4 K [12], we find no indication for superconductivity for the Ce- and Gd-substituted samples. The *RE* substitution seems at least to lower the $T_c$ noticeably.

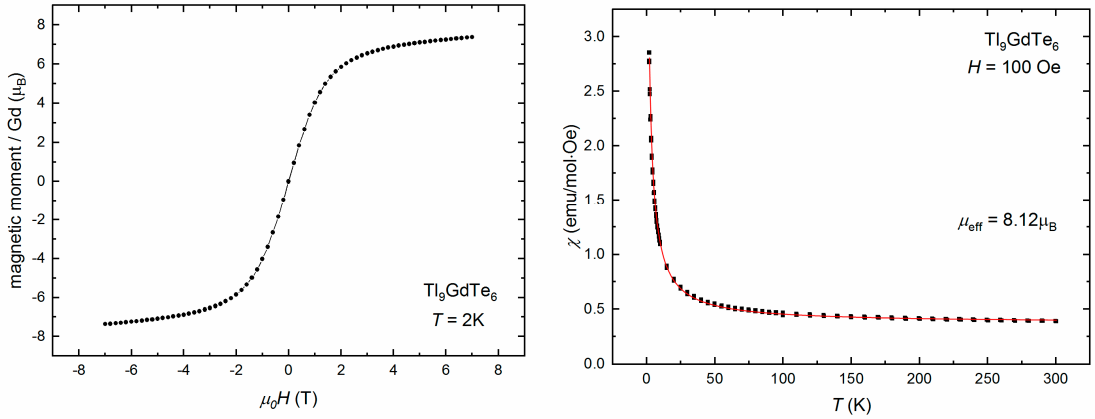


**Figure 7.** $Tl_9GdTe_6$ magnetic moment versus magnetic field for at $T$ = 2 K (left) and magnetic moment vs. temperature for in external fields of 100 Oe (right). The red line depicts the Curie–Weiss fit according to $\chi = A + \frac{C}{T-\theta}$ with $A$: temperature independent correction term for core diamagnetism, Van Vleck contribution and Pauli paramagnetic contribution, $C$ = Curie temperature, $\theta$ = Weiss constant.

## 4. Conclusions

In contrast to previous investigations, the stoichiometrically substituted tellurides $Tl_9CeTe_6$, $Tl_9SmTe_6$ and $Tl_9GdTe_6$ were found to adopt an ordered variant of the $In_5Bi_3$ type, which allows for an adaption of the different metal atom sizes. The compounds crystallize in space group $I4/m$ (no. 87) and the structures can be understood as charge-ordered in accordance with a Zintl-type formula $(Tl^{+})_9RE^{3+}(Te^{2-})_6$. Spin-polarized DFT calculations for $Tl_9GdTe_6$ result in a low, but finite density of states at the Fermi level. The experimental transport behavior determined on hot-pressed powder samples points towards $p$-type semiconductors for the $Tl_9RETe_6$ compounds with relatively high conductivity values at ambient temperature. Our preliminary calculations also indicate a possibility for non-trivial topology of the electronic structure, which will be studied in full detail elsewhere. There is an (avoided) band crossing at the Γ point of the 3D Brillouin zone at ca. 0.2 eV below the Fermi level. Thus, $Tl_9GdTe_6$ may become a candidate topological material upon $p$-doping and given a ferromagnetic ordering. The calculated ground state is ferromagnetic with 7.4 $\mu_B$/Gd-atom, however, magnetization measurements reveal paramagnetic behavior down to 2 K with a moment of 8.12 $\mu_B$/Gd atom. As reported previously, the experimentally derived moment of 2.18 $\mu_B$/Ce atom points to a certain amount of $Ce^{4+}$ in $Tl_9CeTe_6$.

**Supplementary Materials:** The following are available online at http://www.mdpi.com/2073-4352/10/4/277/s1, Table S1: Crystallographic data and refinement parameters of $Tl_9RETe_6$ in space group $I4/mcm$ with Tl1/$RE$ mixed occupancy on Wyckoff site 4*c* of the for reasons of comparison, Figure S1: Profile plots for $Tl_9CeTe_6$, and $Tl_9SmTe_6$ (exp. data and Rietveld fits), Figure S2: Magnetic data for $Tl_9CeTe_6$.

**Author Contributions:** A.I. performed and analyzed the electronic structure calculations. R.S. performed and analyzed the magnetic measurements. T.D. performed and analyzed the powder and single-crystal X-ray data collections, elucidated the crystal structures and supervised the project. All three authors contributed to writing of the manuscript. All authors have read and agreed to the published version of the manuscript.

**Funding:** This research was funded by the Deutsche Forschungsgemeinschaft (grants Do 590/5 and IS 250/1) in the framework of the priority program 1666 "Topological Insulators".

**Acknowledgments:** We are grateful to M. Münch for sample preparations and to A. Brünner for EDX investigations. Open Access Funding by the Publication Fund of the TU Dresden.

**Conflicts of Interest:** The authors declare no conflict of interest.

## References

1. Wölfing, B.; Kloc, C.; Teubner, J.; Bucher, E. High performance thermoelectric $Tl_9BiTe_6$ with an extremely low thermal conductivity. *Phys. Rev. B* **2001**, *86*, 4350–4353.

2. Yamanaka, S.; Kosuka, A.; Korosaki, K. Thermoelectric properties of $Tl_9BiTe_6$. *J. Alloys Compd.* **2003**, *352*, 275–278. [CrossRef]
3. Guo, Q.; Kleinke, H. Thermoelectric properties of hot-pressed $Tl_9LnTe_6$ (Ln = La, Ce, Pr, Nd, Sm, Gd, Tb) and $Tl_{10-x}La_xTe_6$ ($0.90 \leq x \leq 1.05$). *J. Alloys Compd.* **2015**, *630*, 37–42. [CrossRef]
4. Shi, Y.; Sturm, C.; Kleinke, H. Chalcogenides as thermoelectric materials. *J. Solid State Chem.* **2019**, *270*, 273–279. [CrossRef]
5. Sankar, C.R.; Bangarigadu-Sanasy, S.; Assoud, A.; Kleinke, H. Syntheses, crystal structures and thermoelectric properties of two new thallium tellurides: $Tl_4ZrTe_4$ and $Tl_4HfTe_4$. *J. Mater. Chem.* **2010**, *20*, 7485–7490. [CrossRef]
6. Bangarigadu-Sanasy, S.; Sankar, R.; Assoud, A.; Kleinke, H. Crystal structures and thermoelectric properties of the series $Tl_{10-x}La_xTe_6$ with $0.2 \leq x \leq 1.15$. *Dalton Trans.* **2011**, *40*, 862–867. [CrossRef]
7. Kuropatwa, B.A.; Assoud, A.; Kleinke, H. Phase range and physical properties of the thallium tin tellurides $Tl_{10-x}Sn_xTe_6$ ($x \leq 2.2$). *J. Alloys Compd.* **2011**, *509*, 6768–6772. [CrossRef]
8. Sankar, C.R.; Bangarigadu-Sanasy, S.; Kleinke, H. Thermoelectric Properties of $TlGdQ_2$ (Q = Se, Te) and $Tl_9GdTe_6$. *J. Electron. Mater.* **2012**, *41*, 1663–1666. [CrossRef]
9. Bangarigadu-Sanasy, S.; Sankar, C.R.; Schlender, P.; Kleinke, H. Thermoelectric properties of $Tl_{10-x}Ln_xTe_6$, with Ln= Ce, Pr, Nd, Sm, Gd, Tb, Dy, Ho and Er, and $0.25 \leq x \leq 1.32$. *J. Alloys Compd.* **2013**, *549*, 126–134. [CrossRef]
10. Bangarigadu-Sanasy, S.; Sankar, C.R.; Dube, P.A.; Greedan, J.E.; Kleinke, H. Magnetic properties of $Tl_9LnTe_6$, Ln= Ce, Pr, Tb and Sm. *J. Alloys Compd.* **2014**, *589*, 389–392. [CrossRef]
11. Kuropatwa, B.A.; Guo, Q.; Assoud, A.; Kleinke, H. Optimization of the Telluride $Tl_{10-x-y}Sn_xBi_yTe_6$ for the Thermoelectric Energy Conversion. *Z. Anorg. Allg. Chem.* **2014**, *640*, 774–780. [CrossRef]
12. Arpino, K.E.; Wallace, D.C.; Nie, Y.F.; Birol, T.; King, P.D.C.; Chatterjee, S.; Uchida, M.; Koohpayeh, S.M.; Wen, J.-J.; Page, K.; et al. Evidence for topologically protected surface states and a superconducting phase in $[Tl_4](Tl_{1-x}Sn_x)Te_3$ using photoemission, specific heat, and magnetization measurements, and density functional theory. *Phys. Rev. Lett.* **2014**, *112*, 017002. [CrossRef] [PubMed]
13. Bhan, S.; Schubert, K. Kristallstruktur von $Tl_5Te_3$ und $Tl_2Te_3$. *J. Less-Common Met.* **1970**, *20*, 229–235. [CrossRef]
14. Schewe, I.; Böttcher, P.; von Schnering, H.G. The crystal structure of $Tl_5Te_3$ and its relationship to the $Cr_5B_3$ type. *Z. Kristallogr.* **1989**, *188*, 287–298. [CrossRef]
15. Berg, L.G.; Abdul'manov, A.G. Pseudobinary System $Bi_2Te_3$–$Tl_9BiTe_6$. *Izv. Akad. Nauk SSSR Neorg. Mater.* **1970**, *12*, 2192–2193.
16. Voroshilov, Y.V.; Gurzan, M.I.; Kish, Z.Z.; Lada, L.V. Phase equilibria in the Tl-Pb-Te system and crystal structure of $Tl_4B_4X_3$ and $Tl_9B_5X_6$ compounds. *Inorg. Mater.* **1988**, *24*, 1265–1269.
17. Doert, T.; Höffkes, S.; Klein, C.; Böttcher, P. The crystal structures of $AgTl_4Te_3$ and $AgTl_4Te_3$. *Z. Kristallogr. Suppl.* **1991**, *3*, 52.
18. Bradtmöller, S.; Böttcher, P. Darstellung und Kristallstruktur von $SnTl_4Te_3$ und $PbTl_4Te_3$. *Z. Anorg. Allg. Chem.* **1993**, *619*, 1155–1160. [CrossRef]
19. Bradtmöller, S.; Böttcher, P. Crystal structure of molybdenum tetrathallium tritelluride, $MoTl_4Te_3$. *Z. Kristallogr.* **1994**, *209*, 75. [CrossRef]
20. Doert, T.; Böttcher, P. Crystal structure of antimony nonathallium hexatelluride, $SbTl_9Te_6$. *Z. Kristallogr.* **1994**, *209*, 96. [CrossRef]
21. Bradtmöller, S.; Böttcher, P. Crystal structure of copper tetrathallium tritelluride, $CuTl_4Te_3$. *Z. Kristallogr.* **1994**, *209*, 97. [CrossRef]
22. Tokura, Y.; Yasuda, K.; Tsukazaki, A. Magnetic topological insulators. *Nat. Rev. Phys.* **2019**, *1*, 126–143. [CrossRef]
23. Petricek, V.; Dusek, M.; Palatinus, L. Crystallographic computing system JANA2006: General features. *Z. Kristallogr.-Cryst. Mater.* **2014**, *229*, 345–352. [CrossRef]
24. *AZTECH*; Oxford Instruments: Oxford, UK, 2013.
25. *APEX Suite*; Bruker-AXS: Madison, WI, USA, 2013.
26. Sheldrick, G.M. (Ed.) *SADABS*; Bruker AXS: Karlsruhe, Germany, 2002.
27. *DIAMOND 4*; Version 4.6.1; Structure Visualization Software; Crystal Impact GbR: Bonn, Germany, 2019.

28. The Elk FP–LAPW Code, Version 1.4.22. Available online: http://elk.sourceforge.net (accessed on 17 March 2019).
29. Shick, A.B.; Liechtenstein, A.I.; Pickett, W.E. Implementation of the LDA+ U method using the full-potential linearized augmented plane-wave basis. *Phys. Rev. B* **1999**, *60*, 10763. [CrossRef]
30. Bader, R.F.W. *Atoms in Molecules*; Oxford University Press: Oxford, UK, 1990.
31. Shannon, R.D. Revised effective ionic radii and systematic studies of interatomic distances in halides and chalcogenides. *Acta Crystallogr.* **1976**, *32*, 751–767. [CrossRef]
32. Nordell, K.J.; Miller, G.J. Electronic structure, superconductivity, and substitution patterns in $TI_5Te_3$. *J. Alloys Comp.* **1996**, *241*, 51–62. [CrossRef]
33. Blundell, S. *Magnetism in Condensed Matter*; Oxford University Press: Oxford, UK, 2011.